Microfluid Nanofluid
DOI 10.1007/s10404-013-1261-2

RESEARCH PAPER

Multiplexed microfluidic viscometer for high-throughput complex fluid rheology

Deepak E. Solomon · Siva A. Vanapalli

Received: 25 January 2013 / Accepted: 27 August 2013

Abstract We report the first multiplexed microfluidic viscometer capable of measuring simultaneously the viscosity as a function of shear rate for multiple samples. The viscometer is based on a flow-comparator technique where the interface location between co-flowing streams of test and reference fluids is a sensitive function of the viscosity mismatch between the two fluids. We initially design a single microfluidic viscometer and study two different modes of comparator operation—the interface displacement (ID) mode and the interface compensation mode (IC). We find that both modes yield viscosity curves for Newtonian and polymeric fluids that are consistent with a conventional rheometer. Based on the results from the single microfluidic viscometer, we present an operating window that serves as a guide to assess accessible viscosities and shear rates. We then design a 4-plex and 8-plex viscometer based on the ID mode and show that it is capable of reliably measuring viscosity curves for Newtonian fluids, polymeric solutions and consumer products. Collectively, our results demonstrate that the multiplexed viscometer is capable of measuring in a parallel format, viscosities of fluids spanning nearly three orders of magnitude ($\approx 10^{-3}$–1 Pa s) across a shear rate range of $\approx$1–1,000 s^{-1}. We believe our multiplexed viscometer is a low cost and high-throughput alternative to conventional rheometers that analyze samples serially using expensive robotic liquid-handling systems. The multiplexed viscometer could be useful for rapidly analyzing a wide selection of complex fluids on-site during product formulation and quality control.

D. E. Solomon · S. A. Vanapalli (✉)
Department of Chemical Engineering, Texas Tech University, Lubbock, TX 79409-3121, USA
e-mail: siva.vanapalli@ttu.edu

1 Introduction

The rheological properties of complex fluids are of prime importance in various industries such as paints, petroleum and foods (Pal et al. 1992; Larson 1999; Rao 2006; Tadros 2010). Properties such as shear viscosity impact the ability to effectively process and transport complex fluids. Conventional viscosity measurement devices such as rotational rheometers and capillary viscometers are often used to characterize the viscosity of complex fluids in industrial settings. In recent years due to advances in materials and microfabrication technology, several microscale viscometers as well as microfluidic rheometers have been developed. These miniaturized devices have significant potential to be used in various industrial applications because of their small size, cost-effectiveness, ease of use and small sample volume requirements compared to their macroscale counterparts (Pipe and McKinley 2009). The microfluidic viscometers also offer the possibility of point-of-care diagnosis of various medical disorders (Ong et al. 2010).

Microfluidic viscometers developed to date exploit different operating principles to measure viscosity across various regimes of shear rates. Three main operating principles currently exist depending upon how fluids are driven into the microchannels and the means by which pressure drop or flow rate is measured. In one approach, microfabricated pressure transducers (Pipe et al. 2008; Pan and Arratia 2012) or drag force sensors (Noel et al. 2011) are integrated into a microfluidic channel to record directly the pressure drop as a function of imposed flow rate. Flow rates are varied using syringe pumps, and sample viscosity as a function of shear rate is subsequently computed from equations developed for a slit rheometer (Macosko 1994). A significant advantage of this approach is the ability to measure viscosity of complex fluids at very high shear rates

Published online: 13 September 2013

($>10^4$ s^{-1}), which are not easily accessible by conventional rheometry. However, studies (Pipe and McKinley 2009; Pan and Arratia 2012) indicate difficulty in measuring low-viscosity fluids at low shear rates (<50 s^{-1}) due to the minimum pressure drop that can be reliably measured from the pressure sensor.

In a second approach, microfluidic viscometers have been designed using capillary pressure-driven flows (Srivastava and Burns 2006; Han et al. 2007; Tang and Zheng 2011). Known pressure drops are imposed (using the Young–Laplace Law), and the resulting fluid velocity depends on sample viscosity. The mean velocity is computed from the time evolution of fluid imbibition into the microchannel. Interestingly, since the fluid velocity continuously decreases as more sample is imbibed, a wide range of shear rates can be obtained from a single run. Viscosities extracted using this microfluidic capillary viscometer showed good agreement with conventional rheometry. One limitation of this approach is that since imposed pressure drops depend on surface tension of the fluid and wettability of channel walls, it limits the range of viscosities and shear rates that can be accessed. For example, Srivastava and Burns (2006) reported that for very high-viscosity fluids (700–50 mPa s), data could be obtained only at lower shear rates (5–200 s^{-1}), and for very low-viscosity fluids ($\sim$1 mPa s), only higher shear rates (50–1,000 s^{-1}) were accessible. In addition, reusability of a single device for multiple samples may be of concern due to changes in device wettability.

In the third approach, microfluidic devices employing co-flowing laminar streams have been used to measure viscosity (Galambos and Forster 1998; Guillot et al. 2006; Choi and Park 2010; Lan et al. 2010). In this method, typically two fluids, one with known viscosity (reference fluid) and the other with unknown viscosity (test fluid) are allowed to flow next to each other into the so-called comparator region (Groisman et al. 2003; Vanapalli et al. 2007, 2009), where location of the fluid–fluid interface is a sensitive function of the viscosity mismatch between the two fluids. The device geometry consists of either a T-junction (Galambos and Forster 1998; Guillot et al. 2006) or Y-junction (Choi and Park 2010) or a cross-channel (Nguyen et al. 2008). In contrast to other approaches, the implementation of this flow-comparator-based technique is simple, as it does not require microfabricated pressure sensors nor is it limited by surface tension of the fluids. A potential drawback is that diffusion across the interface may preclude accurate quantification of low-viscosity fluids at very low shear rates (Guillot et al. 2006; Nguyen et al. 2008). Using an immiscible fluid as one of the co-flowing streams can alleviate smearing of the interface due to diffusion, but quantification of viscosity becomes cumbersome, as detailed knowledge of the mean curvature of the interface is required (Guillot et al. 2006). In addition, with immiscible fluids, viscosity measurement can only be determined in the jetting regime (Guillot and Colin 2005), which limits range of operation as well as capability for multiplexing.

From a practical perspective, microfluidic viscometers employing different operating principles target specific objectives demanded by applications. For example, the silicon devices integrating on-chip pressure sensors are ideal for obtaining viscosity data at extreme shear rates similar to those found in ink-jet printing. Likewise, the microfluidic capillary viscometer because of its ability to handle very small volumes has the potential for point-of-care clinical diagnostics (Srivastava et al. 2005). Viscometers based on the co-flowing laminar streams have also been exploited to measure intrinsic viscosity (Lee and Tripathi 2005) and aggregation (Choi and Park 2010) in biopolymer solutions.

Despite the existence of various microfluidic viscometers catering to specific applications, a significant unmet need is the capability of current devices to handle multiple samples simultaneously. This multiplexed capability could be potentially useful in screening the viscosity of product formulations for a variety of applications. For example, industries such as those in paints and pharmaceuticals have the need to assess the viscosity of a range of candidate solutions during the development of new products. Alternatively, the formulation of existing products may need to be revised due to factors such as cost, fluctuations in supply and demand, and new guidelines prescribed by regulatory agencies. In either case, multiplexed viscosity measurements might help to rapidly screen a wide selection of formulations.

In this work, we design a multiplexed viscometer based on the operating principle of co-flowing laminar streams in a microfluidic comparator, as this approach scales favorably with increasing number of samples to be tested. We begin by investigating the different modes in which the flow-comparator technique can be used to measure viscosity. Results from this investigation enable us to assess which mode is best suited for multiplexing and also allows us to determine the limits of operation of this technique. Subsequently, we demonstrate a multiplexed microfluidic viscometer capable of measuring viscosity as a function of shear rate of up to 8 samples in a simultaneous manner. We further show the applicability of our multiplexed viscometer to industrial settings, by measuring reliably the viscosity of consumer products including hair gels, mouthwashes and hair sprays simultaneously. Collectively, our results show that the multiplexed microfluidic viscometer is capable of working with a variety of samples with viscosities spanning nearly three orders of magnitude ($\approx 10^{-3}$–1 Pa s) across a shear rate range of $\approx$1–1,000 s^{-1}.

2 Materials and methods

2.1 Sample preparation

We prepared Newtonian fluid samples using 99 % pure glycerine (Sigma-Aldrich, St. Louis, MO), which was diluted to various concentrations (25, 40, 50, 60 wt%) with distilled water (DW). We used two different reference fluids for visualization of the interface −0.1 wt% of 1-μm-diameter fluorescently labeled polystyrene beads (Invitrogen, Carlsbad, CA) in DW and food dye (McCormick, Sparks, MD) diluted to 2 wt% in DW. The viscosity of the reference fluid was increased in some instances using glycerol.

For the non-Newtonian fluids, we used solutions of polyethylene oxide (PEO) with manufacturer reported molar mass of 4×10^6 g/mol (WSR301, Sigma-Aldrich, St. Louis, MO). PEO solutions of concentration ranging from 1,500 to 5,000 ppm were tested in the microfluidic viscometer. The solutions were prepared by adding the polymer powder into DW and gently mixed overnight on a roller (Wheaton science, Millsville, NJ) at 5 rpm to avoid shear-induced degradation. Sample vials were wrapped with aluminum foil to minimize photodegradation.

We also tested commercial products in our multiplexed microfluidic viscometer covering a wide range of fluid viscosities ($\approx$0.001–3 Pa s). The commercial products included in the study were Fructis® hair gels (Garnier, Clichey, France), Acne solution (Burts Bees, Durham, NC), Aussie hair spray (Procter & Gamble, Cincinnati, OH), Facial mist spray (THEFACESHOP, Seoul, South Korea), TreSemme hair spray (Godfrey, St. Louis, MO), John Freida conditioners (Kao Corporation, Tokyo, Japan), Listerine® (Johnson & Johnson, PA) and Scope® mouth wash (Procter and Gamble, Cincinnati, OH).

2.2 Device design and fabrication

In this study, we designed three different comparator-based microfludic viscometer devices. First was a single microfluidic viscometer capable of measuring the viscosity of one fluid. This device was used to test the applicability of the flow-comparator method to measure viscosity and also to assess the limits of operation of this technique. As shown in Fig. 1a, b, the single microfluidic viscometer consists of two fluid entry channels that are connected downstream to form the comparator region. Two geometrical designs of the single microfluidic viscometer were fabricated. In the first design, the width of the entry channels and the comparator channel were $w_e = 400$ μm and $w = 1{,}300$ μm, respectively. The entrance length from inlet to the comparator region was $l_1 = 2$ cm; and the distance spanning the comparator region was $l_2 = 0.72$ cm. The channel heights were uniform, $h = 110$ μm. In the second design, $w_e = 400$ μm, $w = 1{,}300$ μm, $h = 80$ μm, $l_1 = 4$ mm and $l_2 = 2$ cm. For our experiments, we mostly used the first geometric design.

The second device was a 4-plex microfluidic viscometer that contains a microfluidic branching network to deliver reference fluid into four flow-comparator modules as shown in Fig. 1c. The channels in the microfluidic branching network have a width of 300 μm and height of $\sim$110 μm. The flow-comparator had a width, $w = 1{,}050$ μm and the same channel height as the branching network. The third device was an 8-plex microfluidic viscometer whose channels in the branching network and the flow-comparator were identical to that of the 4-plex device, except that the reference fluid was delivered using the branching network into eight comparator modules.

For laminar flows, the minimum entrance length (L_e) for the flow to be fully developed in a channel is given by $L_e = d_h(0.6/(1 + 0.035\mathrm{Re}) + 0.056\mathrm{Re})$ (Macosko 1994) where d_h is the hydraulic diameter defined here as 4× channel cross-sectional area/circumference. The Reynolds number (Re) is defined as $\mathrm{Re} = \rho Q d_h/(w_e h \mu)$, where ρ is the density, μ is the viscosity of the test fluid, and Q is the fluid flow rate in the entry channels. In this work, all the devices had an entrance length $\geq 3L_e$ and Re corresponding to the experiments was $\approx 10^{-3}$–50.

All the microfluidic viscometers were fabricated using standard soft lithography techniques (Xia and Whitesides 1998). Briefly, a mold was made by patterning photoresist (SU-8 2050, Microchem, St. Newton, MA) on a silicon wafer. Poly-dimethyl siloxane (PDMS) (Sylgard, Dow Corning, MI) containing the polymer base and crosslinker in the ratio of 10:1 was poured on the SU-8 mold and baked for 4 h at 60 °C. The resulting PDMS replica was then plasma bonded onto a glass slide using a air plasma cleaner (Harrick Plasma, Ithaca, NY). Dimensions of the microfluidic channels were measured using a scanning electron microscope (UHRSEM, Hitachi, Illinois).

2.3 Experimental procedure

In all of our experiments, we imposed known flow rates at the inlets of the microfluidic viscometer using syringe pumps (PHD2000, Harvard Apparatus, MA). Two different syringe sizes were used: 1-mL syringe (BD, Franklin Lakes, NJ) for shear rates >25 s^{-1} and 100-μL syringe (Hamilton, Reno, NV) for shear rates <25 s^{-1}. An equilibration time of 15–20 min was allowed for lower flow rates (<100 μL/h) and about 5 min for higher flow rates (>100 μL/h). For multiplexed experiments, a syringe pump with a multi-rack accessory (Harvard Apparatus, MA) that can hold up to 16 syringes simultaneously was used.

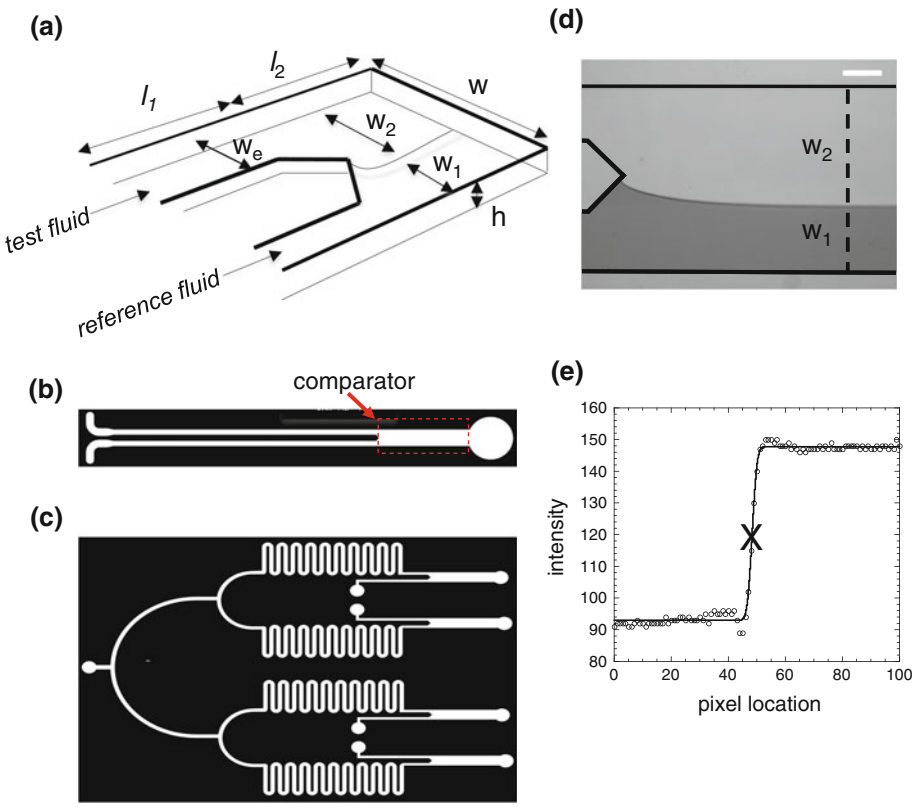

Fig. 1 **a** Schematic of our microfluidic viscometer depicting the longitudinal entrance length (l_1), length and width of the comparator channel (l_2, w), width occupied by the reference fluid (w_1), width occupied by the test channel (w_2) and height of the device (h). **b** Design of the single microfluidic viscometer with inlets for one reference and test fluid. **c** Design of the 4-plex viscometer with a single reference fluid inlet and four test fluid inlets. **d** Image of the microfluidic viscometer in operation. The dyed stream is the reference fluid with width w_1, and w_2 is the width occupied by test fluid. A *dashed vertical line* shows the longitudinal position where widths of the two streams are computed. The *scale bar* represents 250 μm. **e** Plot of pixel intensity (*circles*) along the *dashed vertical line* in (**d**). The *solid line* denotes the computed curve fit, and *X* denotes the 'true' location of the interface

The single and 4-plex devices were used to measure the viscosity of Newtonian (glycerol) and non-Newtonian (PEO) fluids as a function of shear rate. The 8-plex microfluidic viscometer was used to generate viscosity data for eight consumer products simultaneously. The flow rate of the reference stream in the multiplexed viscometer experiments was maintained higher than the test channel flow rate due to the multiple bifurcating channels.

We compared the viscosity data obtained from the microfluidic viscometers with that from conventional macrorheology. Rheological measurements were made on an AR2000 rheometer (TA Instruments, New Castle, DE). All data were collected using a double Couette geometry at a temperature of 23 °C.

2.4 Imaging and interface detection

The images of the interface created by the co-flowing laminar streams in the microchannels were captured with an inverted microscope (IX71, Olympus, Center Valley, PA) using a CCD camera (ImageEM, Hamamatsu, Japan) and a 4x objective (Olympus, Center Valley, PA). Typically, 100 images were acquired to achieve a good statistical accuracy on the location of the interface between the two fluids. Each of the acquired images had a size of 512 × 512 pixels and a spatial resolution of 3.92 μm/pixel.

To detect the interface between the reference and test fluids, as shown in Fig. 1d, an error function was fitted to the intensity profile across the interface at a downstream location where the interface is parallel to the channel walls (Abkarian et al. 2006). In our device, the measurement location is typically 1,000 μm, from the point where the two fluids first meet. The fit used to obtain the 'true location' of the interface is of the form

$$y = a_1 \mathrm{erf}(a_2 x + a_3) + a_4, \quad (1)$$

where y is the range of grayscale values, and a_1, a_2, a_3, a_4 are estimated parameters for the amplitude of the erf function, its slope through the midpoint, the horizontal offset and the vertical offset, respectively. Figure 1e shows the fit of the intensity data to Eq. (1). The midpoint of the position between the lowest and highest gray scale regions

of the fitted curve is taken as the true vertical location of the interface. We find this method yields sub-pixel ($\sim$0.5 pixel) resolution in determining the interface position. Moreover, the interface location was averaged over at least 100 images collected for each experimental run. The image processing was conducted using custom routines written in MATLAB (ver.7.8).

3 Results and discussion

3.1 Basic description of the viscosity measurement technique

The working principle of our microfluidic viscometer is based on two co-flowing laminar streams. As shown in Fig. 2, a fluid of known viscosity seeded with tracer particles is introduced into the reference channel, and the fluid of unknown viscosity is introduced into the test channel. The two fluids are injected at a constant flow rate and meet downstream in the *comparator* region. Depending on how the comparison is made between the two flowing streams, the microfluidic device can be operated in either the interface displacement (ID) or interface compensation (IC) mode as discussed below. We present below the principles underlying these two modes of the flow-comparator operation and discuss how viscosity and shear rate can be determined. In the foregoing discussion, all the variables corresponding to reference and test channels (or fluids) have subscripts of '1' and '2,' respectively.

3.1.1 Two modes of operation of the microfluidic viscometer

In the ID mode, the basic principle is that two co-flowing streams having different viscosities but identical inlet flow rates (Q) occupy different widths of the comparator region as shown in Fig. 2a. This is because, when the inlet flow rates and pressure gradients are the same for the two fluids across the comparator, in order to maintain the same hydrodynamic resistance for each fluid in the comparator region, the stream with higher viscosity occupies a wider portion of the comparator region. For example, as shown in Fig. 2a, when the viscosity of the test fluid is higher than that of the reference fluid, i.e., $\mu_2 > \mu_1$, then the interface displaces downwards, allowing the test fluid to occupy a larger width in the comparator region. To probe the viscosity of the test fluid as a function of shear rate, the flow rate of both the reference stream and test fluid is increased incrementally. The viscosity of the test fluid is quantitatively obtained by knowing the inlet flow rates and measuring the width occupied by each stream from the recorded images and using an analytical theory that describes the flow in the comparator region (discussed in Sect. 3.1.2).

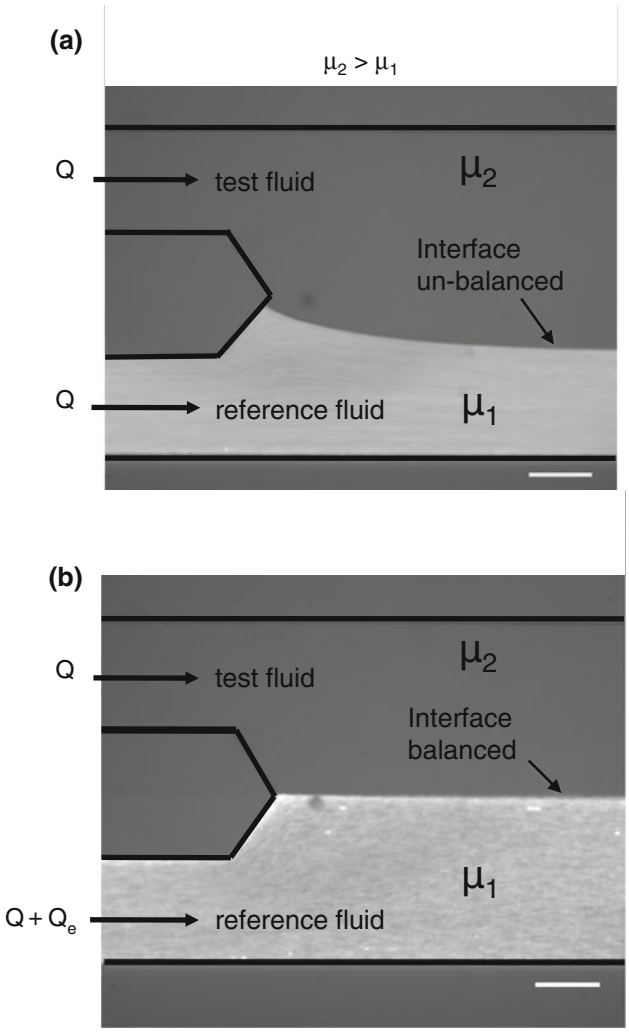

Fig. 2 Working principle of the comparator-based microfluidic viscometer being operated in the **a** Interface displacement mode and **b** Interface compensation mode. The *scale bar* in **a** and **b** is 250 μm

In the IC mode, the viscosity of the test fluid is extracted by balancing the interface so that both the test and reference streams occupy equal widths in the comparator region. For example, if the test fluid occupies a larger portion of the comparator, then the equalization is achieved by increasing the flow rate a compensatory amount (Q_e) to the reference stream to balance the additional resistance offered by the test fluid due to its reduced width as shown in Fig. 2b. Viscosity of the test fluid is measured as a function of shear rate by incrementally varying the test fluid flow rate and balancing the interface by tuning the reference fluid flow rate.

3.1.2 *Quantification of viscosity and mean shear rate in the microfluidic viscometer*

To determine the viscosity of the test fluid and the corresponding mean shear rate, from the inlet flow rates and measured width occupied by one of the streams, we analytically solve the flow field in the comparator region. Our analysis follows that described by Stiles and Fletcher (2004) who solved for the position of the interface between two co-flowing laminar streams in a microchannel using a Fourier series expansion technique. However, Stiles and Fletcher focused on the accuracy of the analytical solution to predict hydrodynamic spreading compared to other numerical simulation techniques. Here, we revisit their analytical results and provide interpretation in the context of (1) viscosity measurement using the two modes of the flow-comparator operation, (2) how the comparator channel aspect ratio influences viscosity measurement and (3) computing the shear rate experienced by the test fluid. We begin by deriving the relationship between the imposed flow rates, viscosity ratio of the two fluids and the comparator channel aspect ratio, for a given location of the fluid–fluid interface.

The domain for solving the flow field in the comparator channel of width (w) and height (h) is shown in Fig. 3a. The reference and test fluids occupy widths w_1 and w_2, respectively. We assume the fluids as Newtonian and incompressible, and for fully developed unidirectional flow, the Navier–Stokes equation for test and reference fluid streams becomes

$$\mu_i\left(\frac{\partial^2 u_i}{\partial x^2}+\frac{\partial^2 u_i}{\partial y^2}\right)=\left(\frac{\partial p}{\partial x}\right)_i \tag{2}$$

where u is the velocity of the fluid in the x-direction, $\left(\frac{\partial p}{\partial x}\right)$ is the longitudinal pressure gradient and index $i = 1, 2$, where 1 and 2 denote quantities pertaining to reference and test fluid streams, respectively.

The kinematic boundary conditions needed to solve Eq. (2) are no-slip boundary conditions at the top and bottom of the channel [Eq. (3)], no–slip at the two sidewalls [Eq. (4)] and velocity continuity at the interface [Eq. (5)]. Note that in Eqs. (3–5), the boundary values for the y and z coordinates are non-dimensionalized by the comparator channel width (w).

$$u_1(y,0) = u_2(y,a) = 0 \tag{3}$$

$$u_1(1/2,z) = u_2(-1/2,z) = 0 \tag{4}$$

$$u_1(Y,z) = u_2(Y,z) \tag{5}$$

In Eq. (3), $a = h/w$ represents the channel aspect ratio, and in Eq. (5), $Y = ½ - w_1/w$ denotes the non-dimensional interface location whose values lies between $-0.5 < Y < 0.5$.

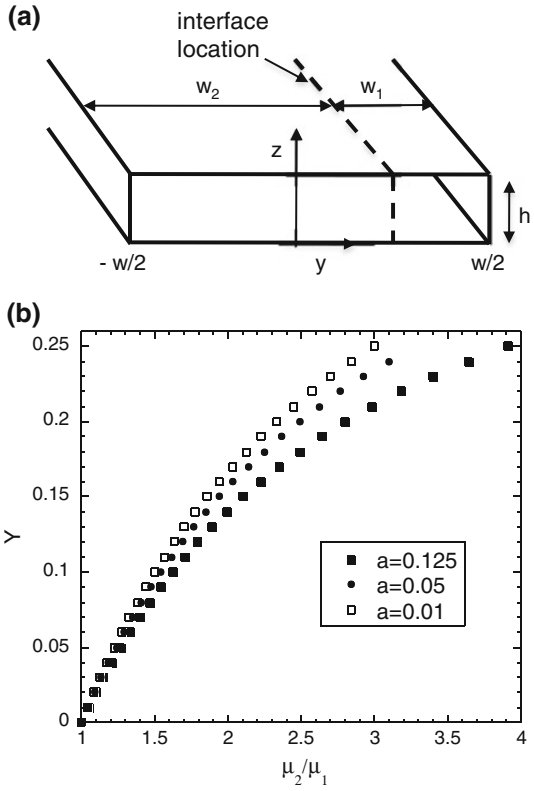

Fig. 3 **a** Domain used for solving the flow in the comparator channel. **b** Interface position as a function of the viscosity ratio as predicted by Eq. (8) for various channel aspect ratios and flow rate ratio of unity

Matching the tangential shear stress and the normal stress at the fluid–fluid interface, we further have Eqs. (6) and (7).

$$\mu_1\frac{\partial \mu_1}{\partial y}\bigg|_Y = \mu_2\frac{\partial \mu_2}{\partial y}\bigg|_Y \tag{6}$$

$$\left(\frac{\partial p}{\partial x}\right)_1 = \left(\frac{\partial p}{\partial x}\right)_2 \tag{7}$$

The solution to Eq. (2) together with the boundary conditions [Eqs. (3–7)] can be obtained using Fourier series expansion (Happel and Brenner 1965). Integrating the velocity profiles in each fluid stream, the ratio of flow rates in the test and reference channel, Q_2/Q_1, can be expressed in terms of three key experimental variables: viscosity ratio μ_1/μ_2, non-dimensional interface location Y and the channel aspect ratio a.

$$\frac{Q_2}{Q_1} = \frac{\mu_1}{\mu_2}\left(\frac{0.5+Y-a\sum_{n=1}^{\infty}\vartheta(v-o\xi\varphi)}{0.5-Y+a\sum_{n=1}^{\infty}\vartheta(\alpha-\xi\tau)}\right) \tag{8}$$

Additional parameters in Eq. (8) are given by

$$q = \pi/2a \tag{8a}$$

$$\vartheta = 48[1 - (-1)^n]/\pi^5 n^5 \tag{8b}$$

$$v = \sinh(2nqY)/\cosh(nq) + \tanh(nq) \tag{8c}$$

$$\alpha = \sinh(2nqY)/\cosh(nq) - \tanh(nq) \tag{8d}$$

$$o = \frac{\tanh(2nqY)\tanh(nq) - 1}{\tanh(2nqY)\tanh(nq) + 1} \tag{8e}$$

$$\xi = \left(\frac{\left(\frac{\mu_2}{\mu_1} - 1\right)\left(\frac{1}{\cosh(2nqY)} - \frac{1}{\cosh(nq)}\right)}{\left(\frac{\mu_2}{\mu_1} + o\right)\tanh(2nqY) + \left(o - \frac{\mu_2}{\mu_1}\right)\tanh(nq)} \right) \tag{8f}$$

$$\varphi = \sinh(2nqY)\tanh(nq) + \cosh(2nqY) - 1/\cosh(nq) \tag{8g}$$

$$\tau = \sinh(2nqY)\tanh(nq) - \cosh(2nqY) + 1/\cosh(nq) \tag{8h}$$

In Eqs. 8b–8h, n denotes the number of terms in the Fourier expansion.

Equation (8) is the key result of the analytical solution that can be used to determine the viscosity of the test fluid in the ID mode. It is apparent from Eq. (8) that the viscosity of the test fluid is a function of the inlet flow rate ratio, interface location and the channel aspect ratio. To understand the influence of these parameters on the viscosity measurement, we plot in Fig. 3b, for a flow rate ratio of unity, the interface position (Y) as a function of the viscosity ratio (μ_2/μ_1) for three different channel aspect ratios. We find that for all aspect ratios, as the viscosity of the test fluid increases, the interface position shifts toward the sidewall of the reference channel, implying more of the comparator region is occupied by the test fluid (to accommodate the higher hydrodynamic resistance of the test fluid due to increased viscosity). The extreme limit of the test fluid fully occupying the comparator channel, i.e., for $Y \to 0.5$, yields the maximum viscosity of the test fluid that can be measured for a given viscosity of the reference fluid. At $Y = 0.49$, our analytical results predict that the maximum contrast in viscosity that can be measured from the ID technique is $\approx$700:1 for a channel aspect ratio of 0.1, although the practical bound may be lower because of the difficulty in measuring accurately the Y value at such extreme interface displacements.

The significance of channel aspect ratio on the viscosity measurement is also reflected in Fig. 3b. The curves of interface position as a function of viscosity ratio change modestly when the channel aspect ratio is increased from 0.01 to 0.125, with no further significant changes occurring for aspect ratios lesser than 0.01. Thus, for truly two-dimensional (2D) comparator channels, the aspect ratio is not a relevant parameter for viscosity determination, in which case, for $a \to 0$, Eq. (8) reduces to the simple form

$$\frac{Q_2}{Q_1} = \frac{\mu_1 w_2}{\mu_2 w_1} \tag{9}$$

Another experimentally relevant observation from Fig. 3b is that in the ID mode, it is best to operate the inlet flow rates in the regime where the absolute Y values are small (i.e., in the middle of the comparator region), because at higher values of Y, small errors in the determination of Y can give rise to large errors in the estimation of viscosity. For example, for a channel aspect ratio of 0.1, at $Y = 0.1$, a 10 % error in determining Y gives an error of 5 % in the viscosity of the test fluid. However, at $Y = 0.35$, a 10 % error in Y produces an error of 60 % in the test fluid viscosity. Moreover, this error in viscosity gets amplified for higher channel aspect ratios.

In the IC mode, the equality of widths occupied by the two streams implies that $Y = 0$. As a result, Eq. (8) reduces to the form

$$\frac{Q_2}{Q_1} = \frac{\mu_1}{\mu_2}\left(\frac{0.5 - a\sum_{n=1}^{\infty}\vartheta(v - o\xi\varphi)}{0.5 + a\sum_{n=1}^{\infty}\vartheta(\alpha - \xi\tau)}\right) \tag{10}$$

For a 2D comparator channel, in the IC mode, Eq. (10) simplifies to

$$\frac{Q_2}{Q_1} = \frac{\mu_1}{\mu_2} \tag{11}$$

We next discuss how the mean shear rate can be obtained from the flow-comparator technique. The mean shear rate experienced by the fluid stream in the test channel in the comparator region is given by

$$\dot{\gamma} = \frac{1}{w_2 h}\int_0^h \int_0^{w_2} \left[\left(\frac{\partial u_2}{\partial y}\right)^2 + \left(\frac{\partial u_2}{\partial z}\right)^2\right]^{1/2} \mathrm{d}y\mathrm{d}z \tag{12}$$

To determine shear rate, we first obtain the velocity profile by solving Eq. 2 for u_2 using the boundary conditions given by Eqs. 3–6 in their dimensional form and truncating the terms in the Fourier expansion to $n = 1$. The calculation for the velocity profile was done in Maple (MapleSoft, Ontario, Canada), and the resulting analytical expression for u_2 was plugged into Eq. (12), which was then solved using the *diff* and *dblquad* function in MATLAB to obtain the mean shear rate.

Because of the ease of computing the viscosity from Eq. (9) [rather than Eq. (8)], it is appealing to design a microfluidic viscometer with a 2D comparator channel. This was indeed the case in the study by Choi and Park (2010), who designed a single microfluidic viscometer with comparator channel of aspect ratio 0.025 and used Eq. 11 to determine the viscosity of protein solutions that behaved as Newtonian fluids over the shear rate range probed (134–941 s^{-1}). However, for a multiplexed viscometer, incorporation of 2D comparator channels leads to a large

footprint and moreover reduces the ability to access lower shear rates. For example, to maintain an aspect ratio of 0.01 (corresponding to the 2D limit), for a comparator channel height of 100 μm, its width needs to be 1 cm, implying that for an 8-plex viscometer, the device footprint will be at least 8 cm. Such large footprint devices can be more prone to channel height variations because of uneven coating of photoresist during spincoating. Thus, in our work, microfluidic comparators with aspect ratios greater than 0.01 were fabricated, and the viscosity was computed explicitly from Eq. (8).

It is also worth to note that applying the 2D analytical results to a non-2D comparator channel geometry may lead to significant errors in the estimation of viscosity. We find that the percentage error in viscosity that one would obtain when applying Eqs. (9, 11) to a non-2D microfluidic comparator grows with increasing aspect ratio (data not shown). Importantly, the error is less for low-viscosity fluids than high-viscosity fluids. In the IC mode, percentage error reaches as high as 15 % for channel aspect ratio of 0.1 and viscosity ratio of 50. In the ID technique for a viscosity ratio of 6, the percentage error reaches as high as 45 % for a similar channel aspect ratio.

Finally, we note that although it may be convenient to operate the multiplexed viscometer by driving fluids using a constant pressure source and manifolds, we find that it is not possible to compute viscosity employing the co-flowing streams. This result can be deduced from Eq. (9), where knowing the pressure drop and viscosity of the reference stream, it reduces to $Q_2\mu_2 = \text{constant}$. Since $Q_2\mu_2 = \text{constant}$, no unique solution (or unique combination of test fluid flow rate and viscosity) exists, implying that a flow-comparator driven by constant pressure boundary conditions cannot be used to quantify fluid viscosity. Physically, this result is due to the fact that co-flowing streams passively maintain the pressure drop between any two vertical locations of the comparator channel by rectifying their widths. This passive rectification is independent of pressures applied at the channel inlets.

3.2 Measurement of viscosity of Newtonian and non-Newtonian fluids using the single microfluidic viscometer

Despite both the ID mode (Galambos and Forster 1998; Guillot et al. 2006) and the IC mode (Choi and Park 2010) being used in the literature, none of the studies have contrasted their capabilities and limits of operation for viscosity measurement. We therefore tested Newtonian and non-Newtonian fluids in the single microfluidic viscometer devices using both the ID and IC techniques. The devices used had comparator channels with aspect ratios of 0.06, 0.085 and 0.122.

In Fig. 4, we show the comparison of the viscometry data generated from the IC technique and ID technique against that from a conventional rheometer, for Newtonian fluids. We note that in Fig. 4, only the mean value of viscosity calculated from the rheometer data is reported as a horizontal line. We find that in general, operating the comparator in either the IC or ID mode yields viscosity data that matches well with the rheometer results. In addition, as expected, both the microfluidic techniques show viscosity to be independent of shear rate for the four Newtonian fluids. Further, we were able to achieve a broad range of shear rates ($\sim$1–6,000 s^{-1}) for some of the fluids. Analysis of data in Fig. 4 also reveals that the IC technique introduces a typical (operator-induced) error of 10–13 % and the ID technique produces an error of $\sim$5–8 %.

Our investigation with Newtonian fluids also revealed the flexibility and limitations associated with each of the modes of operation of the comparator. In the IC technique, the viscosity data deviated significantly from the true value at lower shear rates (<10 s^{-1}) for low-viscosity fluids (see the data for 25 wt% glycerol solution in Fig. 4a). This mismatch is due to diffusion-induced smearing of the interface, which precludes the user from accurately estimating the compensatory flow rate needed to balance the interface. This diffusional broadening of the interface was mitigated for the higher-viscosity fluid (60 wt% glycerol). In striking contrast, diffusional broadening of the interface appears to be negligible in the low shear rate data collected using the ID technique, even for low-viscosity fluids. This significant benefit is due to the flexibility of choosing a relatively higher velocity of the reference fluid compared to the test fluid with the ID technique, which causes a decrease in the residence time of the reference fluid, precluding tracer particles from diffusing across the interface. Thus, operating the microfluidic viscometer in the ID mode yields accurate viscosity at lower shear rates, even for low-viscosity fluids. In fact, we find that our microfluidic viscometer operating in the ID mode provides accurate viscosity data at lower shear rates (1–10 s^{-1}) and at higher shear rates (>2,000 s^{-1}) than a conventional rheometer for 2 mPa s fluid, as shown in Fig. 4c.

There are some limitations in obtaining viscosity data at higher shear rates with both the IC and ID techniques. With the IC technique, we observe that as the viscosity of the fluid increases, data at higher shear rates becomes increasingly inaccessible as shown in Fig. 4a. For example, for 2 mPa s fluid, viscosity data were obtained until shear rates of $\sim$5,000 s^{-1}, whereas for 10 mPa s fluid, viscosity data were limited to shear rates of 600 s^{-1}. This is because, to achieve the same shear rate of 5,000 s^{-1} in the

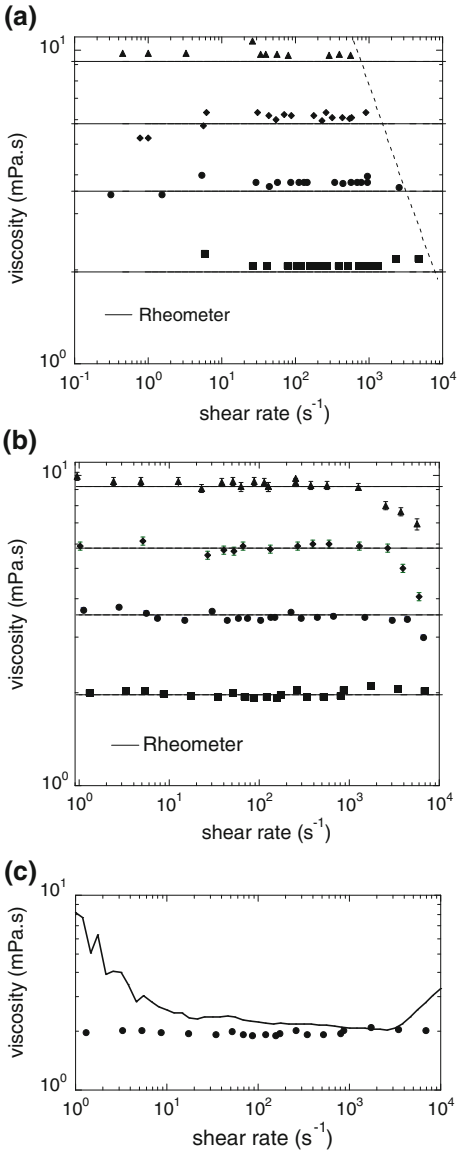

Fig. 4 Validation of the single microfluidic viscometer using Newtonian fluids made with glycerol of concentrations 25 wt% (*squares*), 40 wt% (*circles*), 50 wt% (*diamonds*) and 60 wt% (*triangles*). **a** The *symbols* denote the viscosities of glycerol solutions obtained from the single microfluidic viscometer operating in the interface compensation mode. *Horizontal lines* represent the mean value of viscosity obtained from a rheometer. The *slanted dashed line* indicates region beyond which viscosity data could not be obtained with the interface compensation mode due to device failure. **b** The *symbols* denote the viscosities of glycerol solutions obtained from the microfluidic viscometer operating in the interface displacement mode. *Horizontal lines* represent the mean value of viscosity obtained from a rheometer. **c** Comparison of viscosity as a function of shear rate measured using the rheometer (*solid line*), and our single microfludic viscometer using the interface displacement technique (*symbols*) for a 25 wt% glycerol solution

10 mPa s, the compensatory flow rate needs to be roughly five times higher than that needed for the 2 mPa s fluid [based on the Eq. (11)]. Imposition of such high flow rates with high-viscosity fluids causes our PDMS devices to leak, restricting the accessible range of shear rates with the IC technique. In contrast, the ID technique provides access to higher shear rates than the IC technique (as evidenced by comparing the data in Fig. 4a, b) because of the flexibility in choosing flow rates independently in the test and reference channels.

However, Fig. 4b also shows that the viscosity data can deviate from the true viscosity for higher-viscosity fluids at shear rates beyond those accessible by the IC technique. The reason for this deviation is the formation of a recirculating vortex where the two fluids meet in the comparator region. This flow instability is further discussed in Sect. 3.3. Nevertheless, we find that the ID technique yields reliable viscosity data at shear rates comparable to or higher than that generated from the rheometer.

We next explored the ability of the single microfluidic viscometer to characterize the viscosity of non-Newtonian PEO solutions. To determine viscosity of PEO, we use an approach that is similar to that used in conventional rheometry. For example, in a rotational rheometer, the 'apparent' viscosity curves for non-Newtonian fluids are calculated by assuming Newtonian fluid velocity profile for the fluid contained in the annular gap between rotating cylinders. We also calculate the apparent viscosity of the non-Newtonian fluid by assuming the velocity profile to be that of a Newtonian fluid.

Figure 5 shows the viscosity curves for two concentrations of PEO solutions extracted from our microviscometer. Both the ID and IC techniques yield viscosity data that is in good agreement with that from the rheometer. Since the viscosity of the PEO solutions we chose are markedly higher than that of the Newtonian fluids, diffusional broadening effects were absent, yielding reliable viscosity data at lower shear rates. Moreover, at the lowest shear rate, the convective time scales were about an order of magnitude higher than the diffusion time scales (i.e., Peclet number ≈ 10, based on the diffusion coefficient of water). The dominance of the convective forces indicates that diffusional broadening is minimal, leading to accurate estimates of PEO viscosity (see Fig. 5). Although the viscosity data were in good agreement across the explored shear rate range, one interesting observation was that the level of fluctuations in the interface was markedly higher after a critical shear rate. The inset of Fig. 5b shows that for the 2,500 ppm PEO fluid, the amplitude of interface fluctuations is more at a shear rate of 500 s^{-1}, compared to a shear rate of 100 s^{-1}. These interface fluctuations appear to be consistent with documented elastic instabilities due to co-flowing streams in coaxial cylindrical geometries (Bonhomme et al. 2011) and two fluid layer channel flows (Khomami et al. 2000; Khomami and Su 2000).

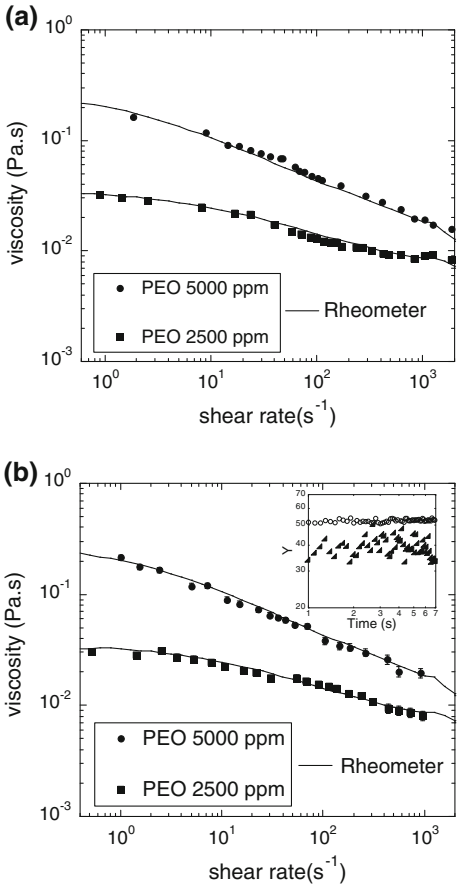

Fig. 5 Viscosity as a function of shear rate for two different concentrations of polymeric PEO fluids obtained from the single microfluidic viscometer using the **a** Interface compensation technique and **b** Interface displacement technique. The *inset* denotes interface position as a function of time for a 2,500 ppm PEO solution at a shear rate of 500 s^{-1} (*triangles*) and 100 s^{-1}(*circles*). The *solid lines* in **a** and **b** denote the viscosity curves from the rheometer

3.3 Operating window of the microfluidic viscometer

Our investigations into viscosity measurement with Newtonian and polymeric fluids have shown that the microfluidic viscometer yields data that agrees well with conventional rheometry. Our experiments also allowed us to identify various phenomena that impose bounds on the range of viscosities and shear rates that can be reliably measured with the comparator-based viscometer technique. These phenomena include (1) diffusion-induced smearing of the interface, (2) device failure due to excessive pressure drops and (3) flow instabilities in the comparator region. We discuss each of these phenomena and establish the operating window for our microfluidic viscometer.

Our results in Fig. 4 show that for low-viscosity fluids at low shear rates, diffusion of tracer particles (or dye) from the reference fluid to the test fluid leads to inaccurate values of viscosity. To estimate the limits in viscosity measurement imposed by diffusion, we determine the average distance (ΔY) traversed by a diffusing tracer particle over a duration corresponding to the fluid residence time (τ) as

$$(\Delta Y)^2 = 2D\tau = \frac{kT}{3\pi\mu_2 r}\tau \tag{13}$$

In Eq. 13, the diffusion coefficient (D) is estimated using the Stokes–Einstein relation, $D = kT/6\pi\mu_2 r$, where k is the Boltzmann constant, T (=296 K) is the absolute temperature, and r (=0.5 μm) is the tracer particle radius. The residence time $\tau = L_\tau/U$, where L_τ (=1,000 μm) is taken to be the longitudinal distance between the location where the two fluids meet first, to the position where the interface location is measured, and U is the velocity scale in the test fluid. Equation 13 assumes one-dimensional diffusion, consistent with the experimental visualization of diffusional broadening along the direction transverse to the flow. Rewriting

$$U = \frac{\dot{\gamma}h}{6}, \tag{14}$$

we get

$$\tau = \frac{6L_\tau}{\dot{\gamma}h} \tag{15}$$

Combining Eqs. (13–15), we derive the diffusion-induced bounds on test fluid viscosity and shear rate as

$$\mu = \frac{2kTL_\tau}{\pi r(\Delta Y)^2 h}\dot{\gamma}^{-1} \tag{16}$$

We plot Eq. (16) in Fig. 6 for typical values of $\Delta Y = 10$ μm and $h = 100$ μm, and the curve shows that for water-like fluids, the lowest shear rate achievable is ≈ 1 s^{-1}. This predicted result based on diffusion across the interface is roughly consistent with our data in Fig. 4. Thus, Eq. 16 could be used as a guide to estimate the lowest viscosity–shear rate combination that can be reliably measured using the comparator-based microfluidic viscometer.

Obtaining viscosity data at higher shear rates can be limited by device failure. In this study, microfluidic devices were fabricated in PDMS and bonded to glass. Depending on the fluid viscosity and shear rates, we observed leakage in the devices due to excessive pressure drops. To estimate the bounds on viscosity and shear rate imposed by such device failures, we quantify the pressure drop due to a flowing liquid in a rectangular PDMS channel, using Eq. (17)

$$\Delta P_{\max} \approx \dot{\gamma}\left(\frac{12\mu_2 L}{h}\right) \tag{17}$$

Taking typical values of the maximum sustainable pressure drop, $\Delta P_{\max} = 10^5$ Pa (McDonald et al. 2000), for

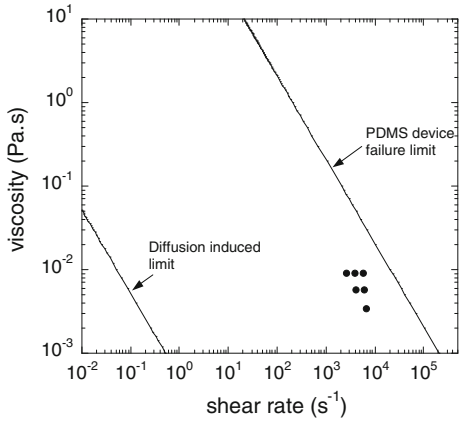

Fig. 6 Operating window of the comparator-based microfluidic viscometer in terms of accessible viscosities and shear rates. The *symbols* denote the experimental conditions where recirculating vortices were observed with Newtonian fluids

a PDMS channel, we plot the dependence of the test fluid viscosity on shear rate (for channel height, $h = 100$ μm and length, $L = 4$ mm) in Fig. 6. We are thus able to quantify the maximum shear rate and viscosity that can be imposed in our PDMS viscometer. Our analysis shows that for a highly viscous fluid sample, the range of shear rates that can be probed are lower compared to the operating shear rate regime for a low-viscosity sample.

Our estimated bounds due to PDMS device leakage may be potentially alleviated by fabricating microfluidic devices in materials much stronger than PDMS (e.g., silicon). However, our study found that flow instabilities may occur below the onset of device failure (see Fig. 6). Previous microfluidic viscometry studies involving the flow-comparator have not identified such instabilities. As illustrated in Fig. 7, streak-line imaging reveals that a recirculating vortex forms in the vicinity of where the two fluids first meet. The data in Fig. 4b show that this instability sets in at lower shear rates (or flow rates) for higher-viscosity test fluids. To gain some qualitative insight into the mechanism of instability, we compute from the data in Fig. 4b, the critical Reynolds number where the onset of instability was observed. We find that for test fluid viscosities of 3.6, 6 and 10 mPa s, the critical Re is 12.9, 4.74 and 1.97, respectively. Thus, our observations suggest that as the viscosity of the test fluid is increased, the critical Re for the onset of this instability *decreases*. We similarly find that the critical flow rate of the test fluid at the onset of instability decreases with increase in fluid viscosity, with an approximate scaling relationship of $Q_2 \sim \mu_2^{-0.9}$. This scaling exponent of about unity suggests that a critical pressure drop across the comparator region may be the determining factor for the onset of the instability, since $\Delta P \sim Q_2\mu_2$. It is well known that when a fluid enters into a channel geometry with contraction and expansion, sudden

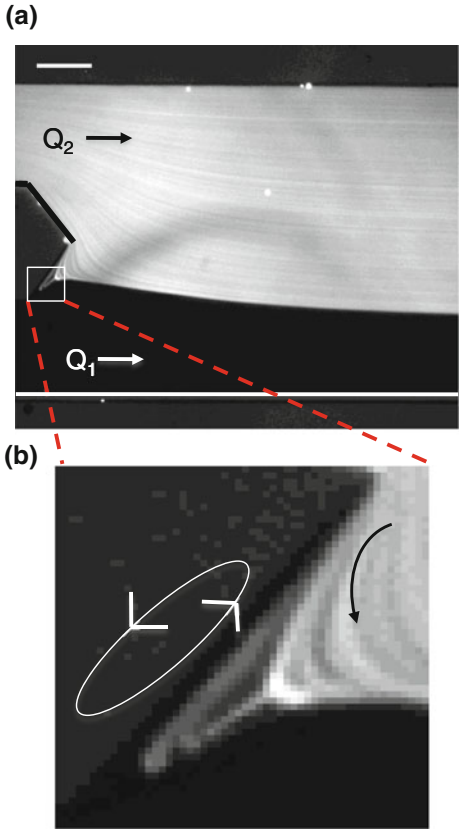

Fig. 7 **a** Image showing a recirculation vortex in the vicinity of where the two fluids meet first in the comparator region. *Scale bar* represents 250 μm. **b** Magnified view of the recirculation vortex. The *arrows* indicate the direction of fluid flow in the region close to the vortex (*black*) and inside the vortex (*white*). The experimental conditions were $Re = 14.2$, $\mu_1 = 1$ mPa s, $\mu_2 = 3.6$ mPa s and $Q_1 = Q_2 = 100$ mL/h

deceleration of the fluid can cause adverse pressure gradients that lead to recirculating vortices. In our geometry, since the test fluid decelerates in the comparator region, similar adverse pressure gradients may arise causing the formation of a recirculating vortex.

3.4 Measurement of viscosity using the multiplexed microfluidic viscometer

Using the single microfluidic viscometer, we have demonstrated that the ID technique is the most flexible method to acquire reliable viscosity over a wide range of shear rates. Also operating the viscometer in the ID mode alleviates manually balancing the interface. We therefore designed a multiplexed viscometer with a single pumping source for the reference fluid that branches into several comparator modules as shown in Fig. 8a.

Several design considerations were taken into account to generate a functional multiplexed viscometer device. Comparator channels of aspect ratio 0.1 were designed to

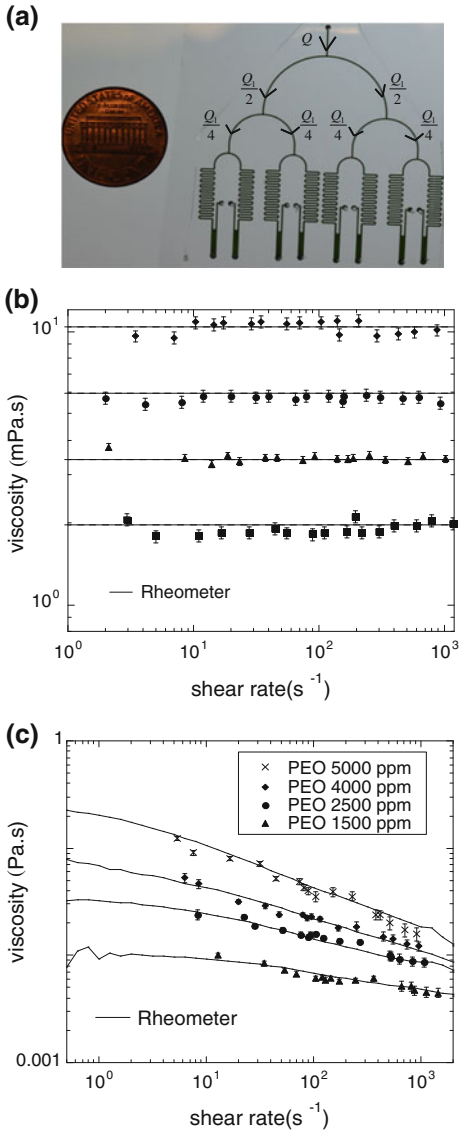

Fig. 8 **a** Image of the 8-plex viscometer showing bifurcating channels to divide the reference fluid into each of the branches. **b** Comparison of viscosities of 25 wt% (*squares*), 40 wt% (*triangles*), 50 wt% (*circles*) and 60 wt% (*diamonds*) glycerol solutions obtained using the 4-plex viscometer and the rheometer. The *symbols* denote the data from the microfluidic viscometer, and *horizontal solid lines* indicate the average viscosity values obtained form the rheometer. **c** Comparison of viscosity of PEO solutions from the 4-plex viscometer (*symbols*) and the rheometer (*solid lines*)

maintain a small footprint of the device. The bifurcating channels were designed to have nearly 50 times higher resistance (by using a serpentine geometry, see Fig. 8a) than the comparator channel. This high upstream resistance ensured equal splitting of the reference fluid flow rate into the bifurcating arms, despite small variations in channel heights. The high upstream channel resistance also prevented 'back flow' of the test fluid into the reference channel from the comparator region.

We first validated our multiplexed device using Newtonian glycerol solutions of various concentrations (Fig. 8b). The viscosities of the Newtonian fluids extracted from this device were in good agreement with the values obtained using a conventional rheometer. The range of shear rates accessible was $\sim$2–1,000 s^{-1}. Attempts to acquire data at shear rates lower than 2 s^{-1} failed because of flow rate fluctuations in the pump that led to unequal splitting of reference fluid flow rates at the bifurcations. The 4-plex viscometer was also used to characterize PEO solutions of four different concentrations simultaneously. Figure 8c shows the viscosity curves for the four solutions, and the data agree well with that from the rheometer.

Finally, we fabricated an 8-plex viscometer to test commercial consumer product samples. The products ranged from low-viscosity fluids such as facial spray to high-viscosity fluids such as hair gels. The commercial samples were loaded into syringes and mounted on a 16-syringe rack attached to the pump. All eight samples were pumped simultaneously into the multiplexed device at a defined flow rate, yielding the product viscosity at one value of shear rate. Figure 9 shows a histogram of the viscosities of the eight samples as measured by the multiplexed viscometer and the rheometer. We observe that the data are in very good agreement, indicating that the multiplexed viscometer could be used to simultaneously characterize viscosity of commercial products.

Although we found good agreement with the commercial fluids chosen in this study, testing of other real-world complex fluids in our device could potentially pose difficulties. Commercial fluids are often multi-component mixtures, which may contain both polar and non-polar ingredients. Measuring the viscosity curves for such complex fluids could become complicated due to partial miscibility of the components into the two fluid streams, leading to interfacial instabilities or inhomogeneous mixing at the interface. In addition, complex fluids can contain mesoscale structures that can also interfere with accurate detection of the interface. Similar to issues present in conventional rheometry, wall slip (Tretheway and Meinhart 2001) and shear banding (Fielding and Wilson 2010) in microchannels may result in non-ideal velocity profiles affecting the viscosity data. Despite these potential issues, which could arise when testing commercial fluids, the data in Fig. 9 suggest that the multiplexed viscometer is capable of measuring viscosity of a variety of complex fluids.

3.5 Comparison of the performance of the multiplexed viscometer with existing high-throughput viscometry techniques

In this work, we demonstrate a multiplexed viscometer that produces viscosity data as a function of shear rate for

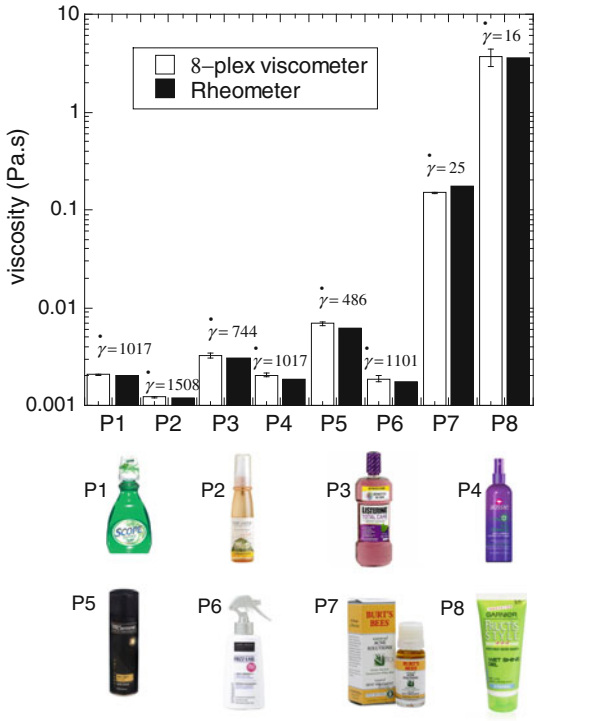

Fig. 9 Viscosity of various consumer products measured simultaneously using the 8-plex viscometer (*open histograms*). The products are mouthwash (*P1*, *P3*), facial spray (*P2*), hair spray (*P4*, *P5*, *P6*), acne solution (*P7*) and hair gel (*P8*). The *solid histograms* represent viscosity data obtained from the rheometer. $\dot{\gamma}$ represents the shear rate at which the data were collected

complex fluids in a high-throughput manner. In the literature, alternative methods have been reported that allow measurement of rheology of several samples simultaneously. In this section, we discuss these methods and contrast their performance compared to our multiplexed viscometer.

A high-throughput version of the falling-ball viscometry was developed by Ma et al. (2008). The method involved simultaneous dropping of millimeter-sized spheres from an adapter mask plate through an array of holes and recording the falling times. The approach was tested for Newtonian fluids, and data were in good agreement with expected values for high-viscosity fluids, but deviated for the low viscosity fluids because of inertial effects. Bead-based microrheology methods have also been extended to high-throughput format. For example, dynamic light scattering has been integrated into multi-well plates for high-throughput viscosity measurements of protein solutions (He et al. 2010). More recently, Schultz and Furst (Schultz and Furst 2011) combined droplet-based microfluidics and particle-tracking microrheology to measure the viscosity of biopolymer solutions.

Although current high-throughput rheology methods cater to specific applications, they do not provide the same capabilities offered by our multiplexed viscometer. For example, the falling-ball viscometry is most suited for Newtonian fluids, and the rheology of complex fluids is difficult to analyze with this technique. Bead-based microrheology methods are capable of measuring viscoelastic moduli of complex fluids under quiescent conditions, but are yet to provide reliable nonlinear rheological properties. The only instrument that is capable of producing viscosity curves for multiple samples similar to our device is the high-throughput rheometer (HTR) commercialized by Anton Paar GmbH (Austria), where a conventional rotational rheometer is instrumented with robotic liquid-handling systems for sample loading and removal. Although fully automated, the HTR is sequential in operation, and we estimate that it requires about 1 h to generate one viscosity curve because of additional time required in loading samples and cleaning the geometry after each run. Our multiplexed viscometer, which is parallel in operation, took 2 h to run eight samples, and another hour for data analysis. Thus, our multiplexed viscometer is about 3 times faster in analysis. It is possible to analyze many more samples than demonstrated without significant increase in measurement time, because of the parallelized format of our viscometer. Finally, our multiplexed viscometer could also be potentially low cost and offers the capability for on-site analysis of multiple samples because of its small device footprint.

4 Conclusions

The goal of this study was to investigate the ability of the flow-comparator technique to measure the viscosity as a function of shear rate for several samples simultaneously. Unlike prior works using the flow-comparator technique to measure viscosity, we assessed the capabilities of the ID mode and IC mode to determine viscosity curves and found that the ID mode is the most convenient and versatile for multiplexed measurements. We also identified previously unreported flow instabilities in the comparator geometry that impose bounds on the range of viscosities and shear rates that can be reliably measured. Recognizing these limits, in Fig. 6, we present an operating window for viscometers that use the flow-comparator technique.

We find that our multiplexed viscometer compares favorably with other high-throughput techniques that produce viscosity curves. Because of the parallelized measurements, analysis time is reduced. With additional automation of both fluid delivery (using syringe pumps) and image acquisition and processing, we expect the throughput to substantially increase. With respect to sample volume requirements, our device requires 1.5 mL of sample for a typical viscosity curve (1–1,000 s^{-1}); however, for single-point viscosity measurements, the sample

volumes needed would be in the microliter range. Our multiplexed viscometer with these benefits could be potentially useful for measuring physical quantities (e.g., intrinsic viscosity of polymer solutions) and screening the viscosity of several samples for industrial applications.

Acknowledgments We thank Dr. Zeina Khan for writing the interface detection code. We are also grateful to Prof. Rajesh Khare for access to rheometer. Acknowledgment is made to the Donors of the American Chemical Society Petroleum Research Fund (PRF No. 50521-DN19) for support of this research.

References

Abkarian M et al (2006) High-speed microfluidic differential manometer for cellular-scale hydrodynamics. Proc Natl Acad Sci USA 103(3):538–542

Bonhomme O et al (2011) Elastic instability in stratified core annular flow. Phys Rev E 83(6):065301

Choi S, Park JK (2010) Microfluidic rheometer for characterization of protein unfolding and aggregation in microflows. Small 6(12): 1306–1310

Fielding SM, Wilson HJ (2010) Shear banding and interfacial instability in planar Poiseuille flow. J Nonnewton Fluid Mech 165:196–202

Galambos P, Forster F (1998) An optical microfluidic viscometer. ASME Int Mech Eng Cong Exp 66:187–191

Groisman A et al (2003) Microfluidic memory and control devices. Science 300(5621):955–958

Guillot P, Colin A (2005) Stability of parallel flows in a microchannel after a T junction. Phys Rev E 72(6):066301

Guillot P et al (2006) Viscosimeter on a microfluidic chip. Langmuir 22(14):6438–6445

Han Z et al (2007) A PDMS viscometer for microliter Newtonian fluid. J Micromech Microeng 17(9):1828–1834

Happel J, Brenner B (1965) Low Reynolds number hydrodynamics. Prentice-Hall, Englewood Cliffs

He F et al (2010) High-throughput dynamic light scattering method for measuring viscosity of concentrated protein solutions. Anal Biochem 399(1):141–143

Khomami B, Su KC (2000) An experimental/theoretical investigation of interfacial instabilities in superposed pressure-driven channel flow of Newtonian and well characterized viscoelastic fluids Part I: linear stability and encapsulation effects. J Nonnewton Fluid Mech 91:59–84

Khomami B et al (2000) An experimental/theoretical investigation of interfacial instabilities in superposed pressure-driven channel flow of Newtonian and well characterized viscoelastic fluids Part II. Nonlinear stability. J Nonnewton Fluid Mech 91:85–104

Lan WJ et al (2010) Rapid measurement of fluid viscosity using co-flowing in a co-axial microfluidic device. Microfluid Nanofluid 8(5):687–693

Larson RG (1999) The structure and rheology of complex fluids. Oxford University Press, New York

Lee J, Tripathi A (2005) Intrinsic viscosity of polymers and biopolymers measured by microchip. Anal Chem 77(22):7137–7147

Ma J et al (2008) High-throughput viscosity determinations. Rev Sci instrum 79(9):094102

Macosko CW (1994) Rheology: principles, measurements and applications. Wiley, New York

McDonald JC et al (2000) Fabrication of microfluidic systems in poly(dimethylsiloxane). Electrophoresis 21(1):27–40

Nguyen N-T et al (2008) Microfluidic rheometer based on hydrodynamic focusing. Meas Sci Technol 19:1–9

Noel MH et al (2011) Viscometer using drag force measurements. Rev Sci Instrum 82(2):023909

Ong PK et al (2010) Are microfluidics-based blood viscometers ready for point of care applications? A review. Crit Rev Biomed Eng 38(2):189–200

Pal R et al (1992) Emulsions fundamentals and applications in the petroleum industry. In: Schramm L (ed) Rheology of emulsions. American Chemical Society, Washington

Pan L, Arratia PE (2012) A high-shear, low Reynolds number microfluidic rheometer. Microfluid Nanofluidics (1613–4982)

Pipe CJ, McKinley GH (2009) Microfluidic rheometry. Mech Res Commun 36(1):110–120

Pipe CJ et al (2008) High shear rate viscometry. Rheol Acta 47(5–6): 621–642

Rao MA (2006) Viscosity of food: measurement and application. Encyclopedia of Analytical Chemistry, Wiley

Schultz KM, Furst EM (2011) High-throughput rheology in a microfluidic device. Lab Chip 11(22):3802–3809

Srivastava N, Burns MA (2006) Analysis of non-Newtonian liquids using a microfluidic capillary viscometer. Anal Chem 78(5): 1690–1696

Srivastava N et al (2005) Nanoliter viscometer for analyzing blood plasma and other liquid samples. Anal Chem 77(2):383–392

Stiles PJ, Fletcher DF (2004) Hydrodynamic control of the interface between two liquids flowing through a horizontal or vertical microchannel. Lab Chip 4(2):121–124

Tadros TF (2010) Rheology of paints, in colloids in paints. Wiley, Weinheim

Tang XJ, Zheng B (2011) A PDMS viscometer for assaying endoglucanase activity. Analyst 136(6):1222–1226

Tretheway DC, Meinhart CD (2001) Apparent fluid slip at hydrophobic microchannel walls. Phys Fluids 14(3):L9–L12

Vanapalli SA et al (2007) Scaling of interface displacement in a microfluidic comparator. Appli Phys Lett 90(11):114109

Vanapalli SA et al (2009) Hydrodynamic resistance of single confined moving drops in rectangular microchannels. Lab Chip 9(7): 982–990

Xia YN, Whitesides GM (1998) Soft lithography. Annu Rev Mater Sci 28:153–184